A novel discrete velocity method for solving the Boltzmann equation including internal energy and non-uniform grids in velocity space

P. Clarke, P. Varghese, D. Goldstein, A. Morris, P. Bauman, and D. Hegermiller

Citation: AIP Conference Proceedings **1501**, 373 (2012); doi: 10.1063/1.4769545
View online: http://dx.doi.org/10.1063/1.4769545
View Table of Contents: http://scitation.aip.org/content/aip/proceeding/aipcp/1501?ver=pdfcov
Published by the AIP Publishing

A Novel Discrete Velocity Method for Solving the Boltzmann Equation Including Internal Energy and Non-Uniform Grids in Velocity Space

P. Clarke[a], P. Varghese[a], D. Goldstein[a], A. Morris[a] , P. Bauman[b], and D. Hegermiller[a]

[a]*ASE-EM Department, The University of Texas at Austin, 210 E 24th St, Stop C0600, Austin, TX 78712, USA*
[b]*ICES, The University of Texas at Austin, 201 E 24th St, Stop C0200, Austin, TX 78712, USA*

Abstract. The discrete velocity method has been extended to include inelastic collisions with rotational-translational energy exchange. A single value of rotational energy per unit mass is assigned to every velocity in the velocity domain and inelastic collisions are modeled using the Larsen-Borgnakke method. The discrete velocity version of energy exchange is used to simulate both a homogeneous relaxation of a distribution with non-equilibrium rotational and translational temperatures and a 1D shock with rotational energy modes. The method has also been modified to allow for non-uniform grids in velocity space. Non-uniform grids permit computational effort to be focused on specific areas of interest within the velocity distribution function. The Bobylev-Krook-Wu solution to the Boltzmann equation (the only analytic solution known) is used to compare a non-uniform grid with a uniform grid.

Keywords: Boltzmann equation, discrete velocity method, Larsen-Borgnakke, non-equilibrium gas flows, non-uniform grids.
PACS: 47.11.-j, 47.45.-n, 47.70.Nd

INTRODUCTION

We expand a discrete velocity method for solving the Boltzmann equation to include velocity domains with non-uniform grid spacing and inelastic collisions between polyatomic molecules with rotational energy. In previous work the discrete velocity method modeled a single species of monatomic, pseudo-Maxwell molecules with isotropic scattering. The Cartesian velocity domain was discretized uniformly in each direction, and each direction had the same spacing. To simulate more complex flows it is necessary to model polyatomic molecules, and rotational and vibrational degrees of freedom must be accounted for during collisions. A phenomenological model was chosen for simulating energy transfers between modes. Direct Simulation Monte Carlo (DSMC), which can be considered the current gold standard, makes use of the Larsen-Borgnakke phenomenological model [1], and the same model has been implemented in our discrete velocity method.

A fine grid resolution is necessary for non-equilibrium distributions due to large gradients in the velocity distribution function. However, fine grid resolution throughout a large velocity domain is computationally expensive. To reduce the expense of simulations, non-uniform grids were developed that allow grid points to be grouped around features of the distribution that require higher resolution. In regions that do not require high resolution, fewer points can be used. A mass, momentum, and energy conserving interpolation scheme for non-uniform grids was implemented for moving post-collision mass back onto the grid. This interpolation is a generalization of a previously described scheme for uniform grids developed by Varghese [2] and implemented by Morris *et al.* [3].

METHOD

The Collision Integral

Taking into account the strict assumptions of monatomic molecules with an isotropic differential cross section in a single species flow with no body forces, the Boltzmann equation can be scaled and discretized with the resulting form:

28th International Symposium on Rarefied Gas Dynamics 2012
AIP Conf. Proc. 1501, 373-380 (2012); doi: 10.1063/1.4769545

$$\frac{\partial \hat{\phi}}{\partial \hat{t}} + \hat{\eta}\frac{\partial \hat{\phi}}{\partial \hat{x}} = \frac{1}{Kn}\sum_{\zeta_{ijk}} \left[\hat{\phi}(\hat{\eta}')\hat{\phi}(\hat{\zeta}') - \hat{\phi}(\hat{\eta})\hat{\phi}(\hat{\zeta}) \right] \hat{g}\sigma_T dV_{\hat{\zeta}}. \tag{1}$$

Where the velocities, $\hat{\eta}, \hat{\zeta}, \hat{g}$ are scaled by a reference velocity: $\eta_r = \sqrt{2k_b T_r / m}$. T_r is a reference temperature, and k_b is Boltzmann's constant. $\hat{\phi}$ is the scaled mass weighted density function, $\hat{g}$ is the relative velocity of a collision, and σ_T is the total collision cross section. For a uniform grid the differential volume, $dV_{\hat{\zeta}}$, is equivalent to β^3, where β is the grid spacing. Finally, the Knudsen number, Kn, is defined as the ratio between a reference mean free path and the characteristic length scale: $Kn = \left(n_r \sigma_r\right)^{-1}$. We define Knudsen number in this way instead of using the more classical definition for scaling purposes. Due to the non-standard scaling, a rescaling must be applied when discrete velocity solutions are compared to DSMC solutions [4].

Molecules are modeled as quasi-particles with fixed velocity and variable mass at each discrete velocity location. Each quasi-particle has a single, fixed velocity which can be represented as a delta function as opposed to a histogram or distribution around the velocity. As collisions occur in the flow, the magnitude of each spike will change but the velocity will remain constant. The collision integral can be evaluated using either a variable hard sphere (VHS) or variable soft sphere (VSS) collision model. In the VHS model, the total collision cross section is defined by the relation $\sigma_T = g^{-\omega}$ where ω is between 0 and 1. A collision parameter of $\omega = 0$ reduces the model to the case of hard spheres and a collision parameter of $\omega = 1$ reduces to the case of pseudo-Maxwell molecules. The scattering angle, χ, is randomly chosen from the range: $0 < \chi < 2\pi$. The VSS collision model is very similar to the VHS model except the scattering angle is adjusted by the VSS parameter, α [5].

In previous work done by Morris *et al.* [4] it was shown how noise inherent to stochastic models could be reduced by applying Baker and Hadjiconstantinou's variance reduction technique to solving the discrete velocity collision integral [8]. The distribution function is split into an equilibrium distribution, $\hat{\phi}_{eq}$, and a deviation from equilibrium distribution, $\hat{\phi}_{dev}$. The decomposition $\hat{\phi} = \hat{\phi}_{eq} + \hat{\phi}_{dev}$ can be substituted into the collision integral, resulting in three separate terms:

$$\begin{aligned} I = &\sum_{\zeta_{ijk}} \left[\hat{\phi}_{dev}(\hat{\eta}')\hat{\phi}_{dev}(\hat{\zeta}') - \hat{\phi}_{dev}(\hat{\eta})\hat{\phi}_{dev}(\hat{\zeta}) \right] \hat{g}\sigma_T dV_{\hat{\zeta}} + \sum_{\zeta_{ijk}} \left[\hat{\phi}_{eq}(\hat{\eta}')\hat{\phi}_{dev}(\hat{\zeta}') - \hat{\phi}_{eq}(\hat{\eta})\hat{\phi}_{dev}(\hat{\zeta}) \right] \hat{g}\sigma_T dV_{\hat{\zeta}} \\ &+ \sum_{\zeta_{ijk}} \left[\hat{\phi}_{eq}(\hat{\eta}')\hat{\phi}_{eq}(\hat{\zeta}') - \hat{\phi}_{eq}(\hat{\eta})\hat{\phi}_{eq}(\hat{\zeta}) \right] \hat{g}\sigma_T dV_{\hat{\zeta}}. \end{aligned} \tag{2}$$

The final term (*eq-eq*) is identically zero because it is the discrete representation of the collision integral over an equilibrium distribution, and equilibrium distributions are unaffected by collisions [6]. The computation of the collision integral for a distribution that is close to equilibrium would normally be dominated by the *eq-eq* term, but by recognizing that it is identically zero, the integral can be calculated with a significant decrease in computational cost. There is also a substantial reduction to noise in the solution for stochastic computation, because one avoids the relatively large "shot-noise" around zero from this term [4].

Internal Energy

The Larsen-Borgnakke model for energy exchange is used to simulate inelastic collisions between polyatomic molecules. The Larsen-Borgnakke model samples from equilibrium distributions of the internal energy and translational energy modes to determine how to reassign the total energy of a collision [5]. The relaxation rate is enforced by only allowing a fraction of molecules to undergo exchanges between their internal and translational modes. Each quasi-particle is processed through an acceptance-rejection method based on the relaxation number, Z_r, where the inverse of the relaxation number, $1/Z_r$, is equivalent to the probability of energy exchange occurring for a particular particle. If neither quasi-particle is chosen to undergo energy exchange, the collision is regarded as elastic and modeled in the same way as collisions between monatomic molecules. However, if one or both of the particles exchange energy between modes, the collision is modeled as an inelastic collision.

Every discrete velocity is assigned a single value of rotational energy representing the average expected energy at a particular velocity. A more realistic approximation would be to assign each velocity a distribution of rotational energies. However, storing multiple values of energy at each velocity increases computational effort and complicates calculations. Future work will address the issue and allow for multiple energy levels to be represented at each velocity.

The discrete velocity version of Larsen-Borgnakke is very similar to the DSMC version of the model. The rotational and translational energy in the collision is grouped into a single total energy and a post-collision value is drawn from the total based on a probability function:

$$P(E_{rot,1}/E_{total}) = \left(\frac{\xi_{rot,1} + (5-2\omega) + \xi_{rot,2} - 4}{\xi_{rot,1} - 2} \left(\frac{E_{rot,1}}{E_{total}} \right) \right)^{\frac{\xi_{rot,1}}{2}-1} \left(\frac{\xi_{rot,1} + (5-2\omega) + \xi_{rot,2} - 4}{(5-2\omega) + \xi_{rot,2} - 2} \left(1 - \frac{E_{rot,1}}{E_{total}} \right) \right)^{\left(\frac{5}{2}-\omega\right)+\frac{\xi_{rot,2}}{2}-1} . \quad (3)$$

Where ξ_{rot} is the number of rotational degrees of freedom. The probability function is derived from equilibrium distributions of translational and rotational energy as explained by Bird [1]. As described in the literature, acceptance-rejection is used to determine the post-collision internal energy of each molecule when the number of internal degrees of freedom is not equal to 2. When there are two rotational degrees of freedom, the equation $E'_{rot} = E_{total}(1 - R_0^{1/(2.5-\omega)})$, where R_0 is a random number uniformly distributed on [0,1], can be directly applied to calculate the transfer of energy between modes.

The probability equations used in DSMC are formulated for a continuous velocity distribution function, i.e. mass can travel at any velocity. However, in the discrete velocity model, collision pairs are drawn from a fixed set of velocities. Drawing collisions from a discrete, equilibrium velocity distribution may result in a different average translational energy than predicted by the Larsen-Borgnakke probability equations. Energy is then transferred to or from rotational modes to account for the difference, and a slight separation occurs between the final rotational and translational temperatures. As the grid size is decreased the separation also decreases, converging to the correct solution.

Each molecule's post-collision internal energy is removed from the total energy in the collision, leaving a resultant translational energy for the collision pair. Transfer of rotational energy to translation, for example, increases the diameter of the collision sphere, as indicated in figure 1. After the relative velocity vector is rotated, it is elongated to account for an increase in translational energy or shortened to account for a decrease in translational energy.

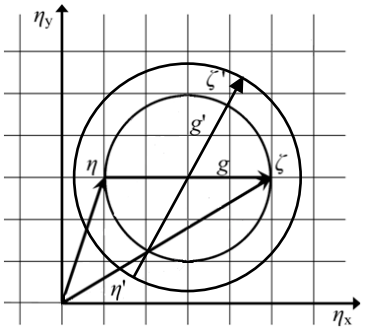

FIGURE 1. Schematic of the post-collision relative velocity vector with energy transfer from rotational modes to translation. The vector is first rotated about the center of mass as prescribed by the collision model then elongated to account for an increase in translational energy. If the translational energy decreases, the vector would be shrunk instead.

Non-uniform Grids in Velocity Space

Non-uniform grids in velocity space may be used to concentrate points where they are most needed. In the current model, the velocity domain may have varying grid point separation, but the grid cannot (yet) change over time. Grid lines can be stretched or shrunk, the domain size changed, or grid lines added or removed, but the current model does not support nested points or non-Cartesian grids. The points can be arranged based on high mass regions of the distribution function, where the distribution function has the largest gradients, in high velocity areas, or based on a variety of other factors. The optimal distribution of points in velocity space is presently unclear (and unexplored). Further, it should be noted that the best configuration to represent the distribution function as a whole might not be the same as the best grid configuration to solve for a particular quantity of interest (say, a chemical rate).

After the relative velocity vector has been rotated according to either the VHS or VSS collision model, there is a very low probability the endpoints will lie exactly on the grid or be symmetrically spaced from the nearest grid points. The asymmetry between the two endpoints forces the interpolation of each mass to be decoupled from the

other. The first step in interpolation is creating a stencil around each post-collision velocity consisting of an origin, three interior points, and three exterior points. A single exterior point is all that is necessary to enforce conservation during interpolation, but three points are chosen for symmetry. If an extra *interior* point is used instead, the resulting matrix becomes singular.

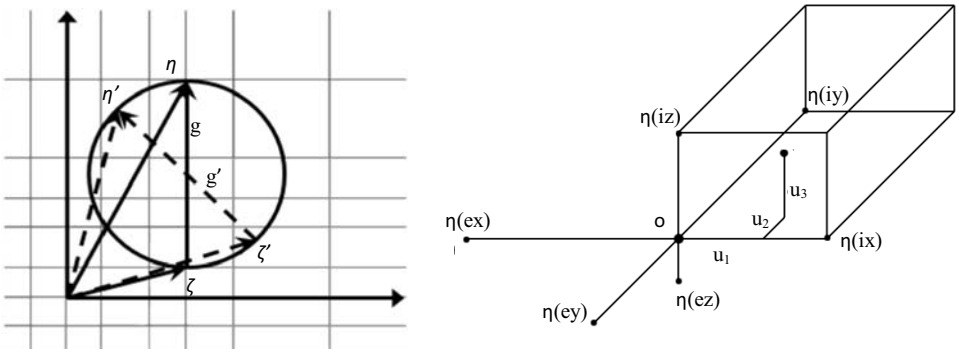

(a) (b)

FIGURE 2. (a) Rotation of the relative velocity vector on a non-uniform grid. Note the lack of symmetry between the two resulting endpoints. (b) Interpolation stencil with non-uniform grid spacing between velocity points.

Taking the five conservation equations (mass, energy, and momentum in each direction), a system of five equations with seven unknowns is described. To solve the system, it is necessary to couple the exterior points. Three natural solutions appear for determining the quantity of mass to move to each exterior point. The amount interpolated can be chosen such that either mass, momentum, or energy is equal at the external points. A uniform grid specific form of the equations was presented in Varghese [2] where the three options for exterior points reduce to the same equation. A more general derivation of the equations can be formed from conservation equations:

$$\Delta_o + \Delta_{i,1} + \Delta_{i,2} + \Delta_{i,3} + \Delta_{e,1} + \Delta_{e,2} + \Delta_{e,3} = 1. \tag{4}$$

$$\Delta_{i,1}\eta_{i,1} + \Delta_{e,1}\eta_{e,1} = u_1. \tag{5}$$

$$\Delta_{i,2}\eta_{i,2} + \Delta_{e,2}\eta_{e,2} = u_2. \tag{6}$$

$$\Delta_{i,3}\eta_{i,3} + \Delta_{e,3}\eta_{e,3} = u_3. \tag{7}$$

$$\Delta_{i,1}\eta_{i,1}^2 + \Delta_{i,2}\eta_{i,2}^2 + \Delta_{i,3}\eta_{i,3}^2 + \Delta_{e,1}\eta_{e,1}^2 + \Delta_{e,2}\eta_{e,2}^2 + \Delta_{e,3}\eta_{e,3}^2 = u_1^2 + u_2^2 + u_3^2. \tag{8}$$

Here Δ is the fraction of $\Delta\hat{\phi}$ interpolated to a point, η_e, η_i are the relative external and internal velocities respectively, and u_1, u_2, and u_3, are the post-collision relative velocities. When the equal external mass constraint is used, the restriction $\Delta_{e,1} = \Delta_{e,2} = \Delta_{e,3} \equiv \Delta_e$ is applied to couple the exterior points. The definition results in the following equations for the ratio of mass sent to each exterior and interior point.

$$\Delta_e = \frac{\sum_{j=1}^{3}\left[u_j\left(u_j - \eta_{i,j}\right)\right]}{\sum_{j=1}^{3}\left[\eta_{e,j}\left(\eta_{e,j} - \eta_{i,j}\right)\right]}, \quad \Delta_{i,j} = \frac{u_j - \eta_{e,j}\Delta_e}{\eta_{i,j}}. \tag{9}$$

For the case of equal external momentum, $\eta_{e,1}\Delta_{e,1} = \eta_{e,2}\Delta_{e,2} = \eta_{e,3}\Delta_{e,3} \equiv M$ is used. We begin by solving for the external momentum:

$$M = \frac{\sum_{j=1}^{3}\left[u_j\left(u_j - \eta_{i,j}\right)\right]}{\sum_{j=1}^{3}\left(\left|\eta_{i,j}\right| + \left|\eta_{e,j}\right|\right)}. \tag{10}$$

Substituting M into the conservation equations results in equations for each exterior point and interior point:

$$\Delta_{e,j} = \frac{M}{|\eta_{e,j}|}, \quad \Delta_{i,j} = \frac{u_j + M}{|\eta_{i,j}|}. \tag{11}$$

Similarly, if we instead specify equal relative kinetic energy, we have: $\eta_{e,1}^2\Delta_{e,1} = \eta_{e,2}^2\Delta_{e,2} = \eta_{e,3}^2\Delta_{e,3} \equiv E$ where

$$E = \frac{\sum_{j=1}^{3}\left[u_j\left(u_j - \eta_{i,j}\right)\right]}{3 - \sum_{j=1}^{3}\left[\frac{\eta_{i,j}}{\eta_{e,j}}\right]}. \tag{12}$$

$$\Delta_{e,j} = \frac{E}{\eta_{e,j}^2}, \quad \Delta_{i,j} = \frac{u_j - \Delta_{e,j}}{\eta_{i,j}}. \tag{13}$$

For all three cases, the mass interpolated to the origin is simply determined from the conservation of mass equation:

$$\Delta_o = 1 - \sum_{j=1}^{3}\left(\Delta_{i,j} + \Delta_{e,j}\right). \tag{14}$$

If a post-collision velocity lies outside or near the velocity domain boundary such that the stencil origin resides on that boundary, three external points will not be available. The system of equations above must be rewritten for configurations of one or two external points. It was noted above that only one exterior point is actually needed to satisfy the conservation equations so the interpolation equations can be obtained using the same method as above.

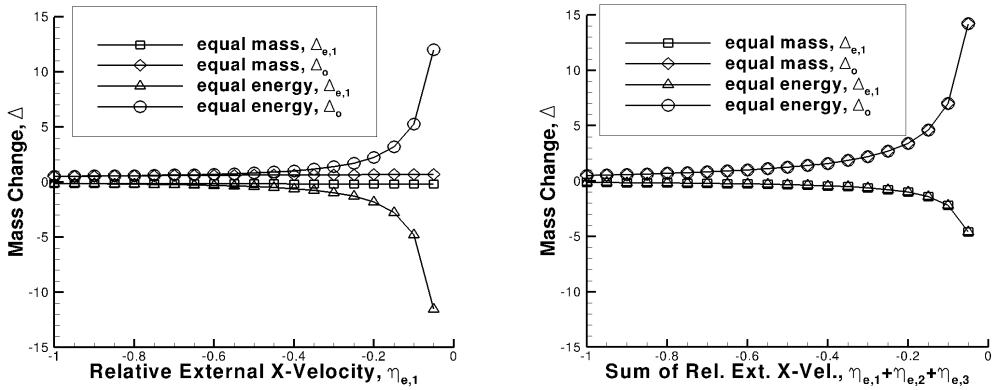

FIGURE 3. (a) Comparison of equal mass and equal energy interpolation choices - fraction of mass interpolated to *x*-external point and origin as *x*-external point is moved closer to the origin. (b) Fraction of mass interpolated to x-external point and origin as all external points are moved closer to origin.

The three methods for interpolation to external points were investigated. An interpolation stencil was created and the distance for the external point relative velocity was varied. As can be seen in figure 3a, the equal energy case produced a singularity as a single external point was moved closer to the origin. A large reduction of mass occurred at the external point and a large increase of mass occurred at the origin of the stencil. These large changes in mass distort the distribution function, producing inaccuracies in the higher moments. However, the equal mass scheme did not produce the singularity as a single external point was moved closer to the origin. Next, all three external points were moved towards the origin at the same time (Figure 3b). Both schemes produce a singularity as the sum of the relative external point velocities approaches zero. The equal momentum case (not shown in Figure 3) follows the same trend as the equal energy case. Due to its less restrictive nature, the equal mass scheme was implemented in the discrete velocity method. Since a singularity still exists, a stretching factor limitation was implemented of 200%. Meaning grid spacing between points cannot be greater than double the grid spacing in the adjacent cells.

RESULTS

Internal Energy

The internal energy method described above has been applied to the discrete velocity model for both a homogeneous relaxation where a Maxwellian is initialized with different translational and rotational temperatures and a 1-D shock case. Comparisons are made to theoretical approximations and equivalent DSMC results produced from Bird's code as described in [1]. For both simulations, N_2 is used as the test gas.

TABLE 1. Relevant properties for N_2

Gas Property	Value
Diameter	4.17×10^{-10} m
Mass	4.65×10^{-26} kg
degrees of freedom, ξ	2
VHS parameter, ω	0.74
Relaxation rate, Z_r	5.0

In the case of homogeneous relaxation shown in figure 3, the distribution is initialized with a scaled translational temperature, $T_{tr} = 1.667$ and rotational temperature, $T_{rot} = 0$. As molecules collide, translational energy is transferred into the internal rotational energy modes. The velocity grid is uniformly spaced with $\beta = 0.4$ and the domain boundary is located at $\hat{\eta} = \pm 4.0$. The scaled time step was $\hat{t} = 0.1$.

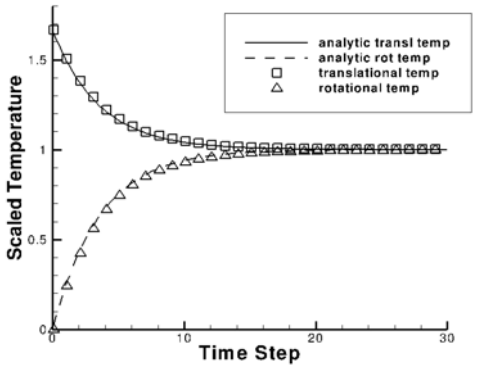

FIGURE 4. Homogeneous relaxation starting from a Maxwellian with T_{tr} = 1.667 and T_{rot} = 0. The solution (symbols) is compared to an analytic relaxation (line).

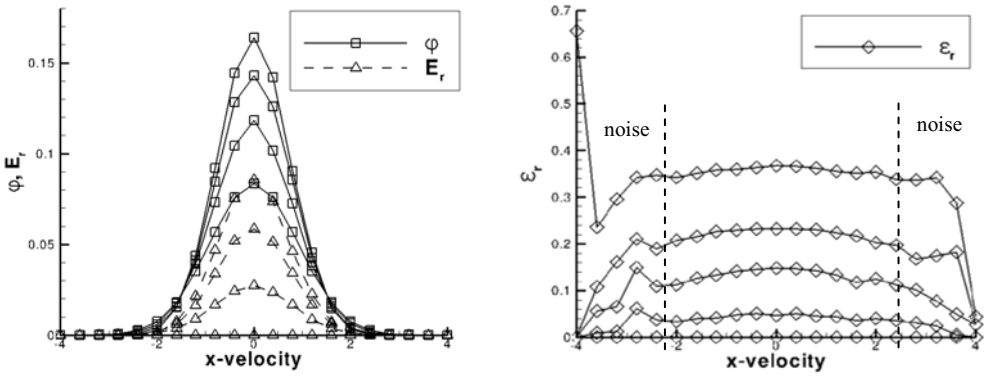

(a) (b)

FIGURE 5. (a) Evolution of the velocity and rotational energy distribution functions through the relaxation. The velocity distribution becomes taller and thinner as the distribution is cooled. (b) Rotational energy per unit mass increases uniformly except in the wings where few collisions occur.

Figure 4 shows good agreement between an analytical approximation of the relaxation and the modeled relaxation. The final rotational temperature is 299.85 K and the final translational temperature is 300.06 K. Velocity distribution functions are easily produced using the discrete velocity method code. As expected, the velocity distribution function becomes narrower as the translational temperature drops when energy is transferred to rotational modes. Note that the Gaussian shaped distributions of rotational energy in figure 5a arise because the distribution plotted is mass weighted. When rotational energy per unit mass is plotted, the energy distribution is expected to be constant across the domain and increase uniformly as energy is transferred to rotational modes. Because the majority of the collisions occur between quasi-particles of lower velocity in the current model, the rotational energy at high velocity values tend to have high noise and lag slightly behind during the relaxation. This has little effect on bulk properties because of the very small population in the tails of the velocity distribution.

A 1-D shock is simulated with a specular left wall and a constant in/out condition at the right wall (figure 6). An initial translational and rotational temperature of 1.0 and an initial scaled upstream velocity of –1.5 are used. The numerical scheme gives a shock that moves to the right at Mach 2.6 when it achieves steady state. The convection step is performed using a 4^{th} order finite difference scheme [7]. In order to compare the solution to a DSMC solution, we freeze the moving shock at a fixed location and compare the shock to a stationary one produced by Bird's DSMC code [1]. The shock shows good agreement in thickness and energy relaxation rate. The discrete velocity method has a very clean upstream and downstream solution. The DSMC solution reaches a slightly higher translational temperature behind the shock, resulting in the small discrepancy between the DVM and DSMC rotational temperatures behind the shock.

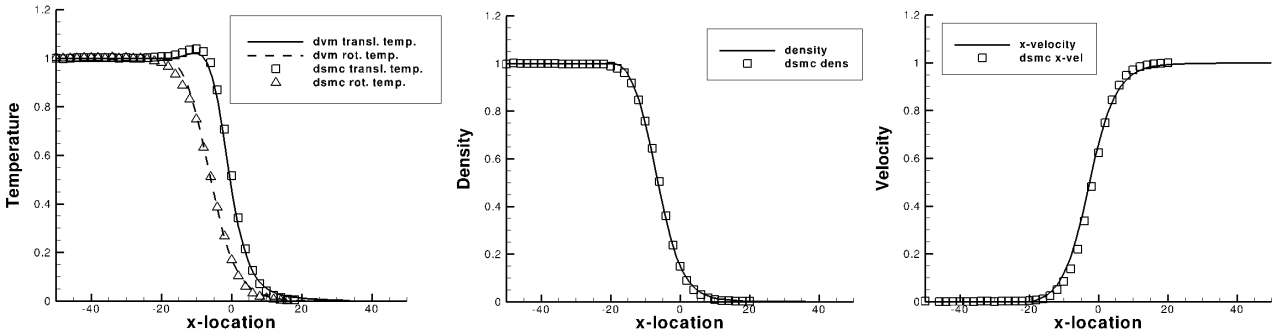

(a) (b) (c)

FIGURE 6. (a) Temperature profiles for a Mach 2.6 shock compared to DSMC. Translational and rotational temperatures are shown. (b) The density profile and (c) velocity profile are compared to DSMC as well.

Non-uniform Velocity Grid

A BKW distribution with a scaled temperature of 1.0 and a density of 1.0 is relaxed using a non-uniform grid and compared to the solution for two different uniform grids. The 4^{th} and 6^{th} moments are plotted to compare the accuracy of each grid (Figure 7). Initially, a fine uniform grid ($\beta = 0.5, \eta = \pm 4.5$) is used for the relaxation. When scaled by the analytic solution [8,9], the fine grid represents the 4^{th} and 6^{th} moments very well. Next, a coarse uniform grid ($\beta = 0.9, \eta = \pm 4.5$) is used. The coarse grid has a very poor approximation of the BKW distribution function and provides an inaccurate result for the 4^{th} and 6^{th} moments during relaxation, but the computations on the coarse grid are performed ~2.5 times faster. Finally, the coarse grid was realigned in the domain ($\eta = \pm 4.5$) such that points were clustered about the center of the distribution. When the BKW distribution was relaxed, much better agreement can be seen in the higher moments, and the speed-up seen for the coarse grid is nearly maintained.

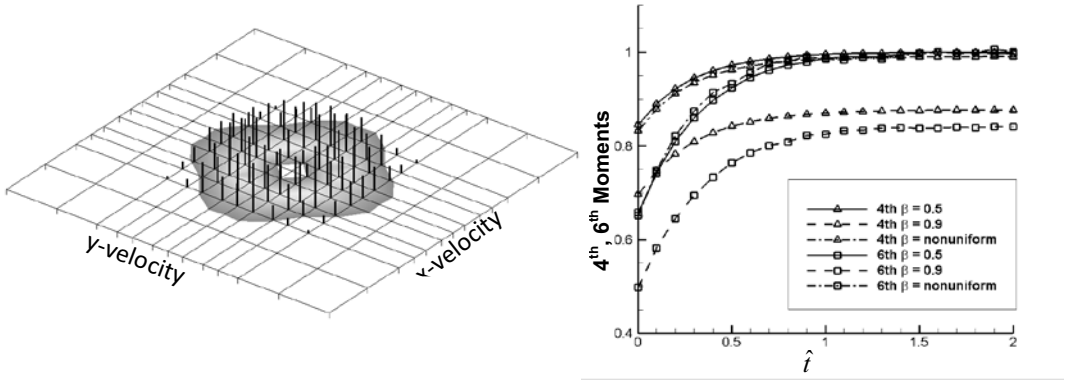

(a) (b)

FIGURE 7. (a) Slice of a BKW distribution on a non-uniform grid. Points are clustered near the center of the domain. (b) 4th and 6th moments during relaxation of the BKW distribution on a non-uniform grid compared with a fine uniform grid and a coarse uniform grid.

CONCLUSIONS

We have implemented polyatomic molecules in the discrete velocity method for solving the Boltzmann equation by simulating inelastic collisions with the Larsen-Borgnakke model. We solved a homogeneous relaxation with an initial translational temperature and no rotational temperature and a 1D shock at Mach 2.6. The homogeneous relaxation shows good agreement with a theoretical approximation and the 1D shock is comparable to DSMC. Non-uniform grids in velocity space were implemented. A more general interpolation scheme was needed to move post-collision mass back onto the velocity grid while conserving mass, momentum, and energy. Given three options for how to determine mass at an exterior point of the interpolation stencil, it was seen that splitting the mass equally between the points was the preferable method. However, the amount a grid can be stretched is still restricted. Velocity grids stretched 200% or less show accurate results when compared to the uniform case. Implementation of non-uniform grids was tested on the BKW relaxation. A fine grid, coarse grid, and non-uniform grid on equal domains were used for the relaxation. The non-uniform grid produces a more accurate result than the coarse grid while maintaining the reduced coarse grid's speed-up in computational time.

ACKNOWLEDGMENTS

We gratefully acknowledge support from NASA under project number NNX11AM72H. The research was also partially supported by the DOE National Nuclear Security Administration under award number DE-FC52-08NA28615.

REFERENCES

1. G. Bird, *Molecular Gas Dynamics and the Direct Simulation of Gas Flows*, Oxford: Oxford Univ. Press. (1994).
2. P. L. Varghese, *RGD: Proc. of the 25th Intl. Symposium*, edited by M.S. Ivanov and A.K. Rebrov, , Novosibirsk, Russia, pp. 227-232, 2007.
3. A. Morris, P. Varghese, D. Goldstein, *RGD: Proc. of the 26th Intl. Symposium*, edited by T. Abe, Kyoto, Japan, AIP Conference Proceedings 1084, American Institute of Physics, Melville, NY, 2009, pp. 458-463..
4. A. B. Morris, P. L. Varghese, and D. B. Goldstein, *J. Comput. Phys.* **230**, 1264-1280 (2011).
5. W. Vincenti and C. Kruger, *Introduction to Physical Gas Dynamics,* John Wiley & Sons (1965).
6. L. Baker and N. Hadjiconstantinou, *Phys. Fluids* **17**, 051703, 1-4 (2005).
7. Z. Tan and P. L. Varghese, *J. Comput. Phys.* **110,** 327-340 (1994).
8. A. V. Bobylev, *Sov. Phys. Dokl.* **20**, 822-824 (1976).
9. M. Krook and T. Wu, *Phys. Fluids* **20**, 1589-1596 (1977).